Chemical tools to modulate endocannabinoid biosynthesis

Deng, H.

7

Activity-based protein profiling reveals the mitochondrial localization of monoacylglycerol lipase

Based on
H. Deng, D. M. van Elsland, A. C. M. van Esbroeck, T. van der Wel, H. den Dulk, H. S. Overkleeft, S. I. van Kasteren, M. van der Stelt; *manuscript in preparation*

Introduction

Activity-based probes (ABPs) are versatile chemical tools to monitor enzyme function in a wide range of biological systems.[1] ABPs are small molecules that covalently and irreversibly inhibit enzymes and that are equipped with a tag (e.g., fluorophore or biotin) through which the target enzyme, or enzyme family, is visualized in living systems by fluorescence microscopy, or enriched to enable identification and characterization using chemical proteomics methodology by mass spectrometers. To date, various ABPs have been designed to target a number of enzyme families, such as serine hydrolases,[2,3] cysteine proteases,[4] phosphatases,[5] kinases,[6] glycosidases,[7] metalloproteases[8] and various oxidoreductases.[9] These ABPs can been used for various applications, including target discovery, (sub)cellular target localization, characterization of enzyme active sites, inhibitor discovery, lead optimization and target engagement.[10] Most of the existing ABPs target numerous enzymes within a family, enabling the global profiling of many enzymes in parallel. Thus, those ABPs

provide a robust method to evaluate the potency and proteome-wide selectivity of inhibitors in a single experiment. Tailor-made ABPs, on the other hand, target only a single enzyme. This provides additional advantages, including visualization of active enzymes in cells, tissues and even animals. The development of such selective tailor-made ABPs poses substantial challenges. Excellent physico-chemical and biological properties, such as solubility, selectivity, cell permeability and pharmacokinetics, are important criteria to apply tailor-made ABPs to living biological systems. Currently, there are only a limited number of tailor-made ABPs available to study enzyme activity in cellular imaging studies.[9,11,12]

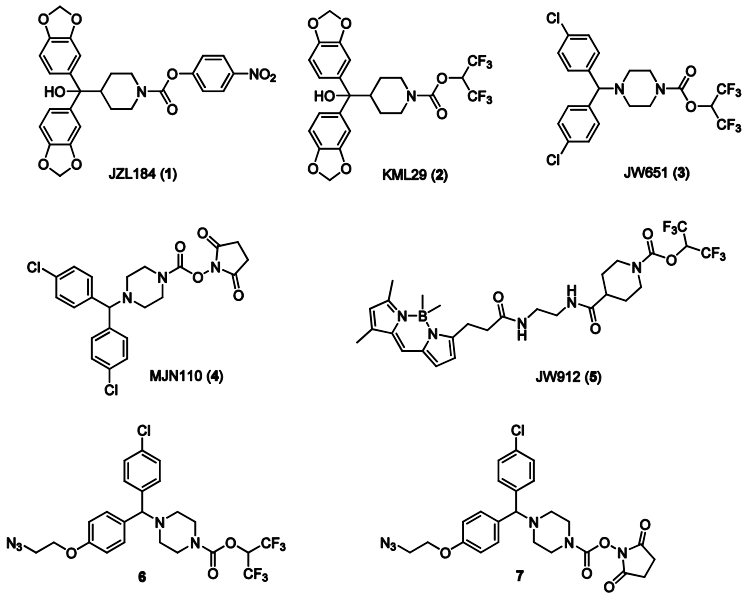

Figure 1. Chemical structures of known MAGL inhibitors **1**-**4** and ABP **5**, and clickable probes **6** and **7** described in this chapter.

Monoacylglycerol lipase (MAGL) is a membrane-associated serine hydrolase, which exists in two splice forms with molecular weight of 33 and 35 kDa, respectively.[13] MAGL links endocannabinoid and eicosanoid biology via hydrolysis of the endocannabinoid 2-arachidonoylglycerol (2-AG), thereby releasing glycerol and arachidonic acid (AA). The latter is the precursor of pro-inflammatory eicosanoids.[14] Additionally, Nomura *et al.* found that MAGL is highly expressed in aggressive human cancer cell lines and primary tumours,[10] where it regulates an oncogenic signaling network of lipids that promotes cancer cell migration, invasion, survival and tumor growth. Consequently, inhibitors of MAGL are proposed to have therapeutic potential as anti-cancer drugs. Several covalent, irreversible MAGL inhibitors (**1**-**4**) and an ABP (**5**) have been reported in the literature (Figure 1). These agents are, however, not

completely selective, which hampers the interpretation of the biological results obtained with these compounds. A common off-target of these inhibitors is the serine hydrolase α,β-hydrolase domain 6 (ABHD6), a lipase that metabolizes various classes of lysophospholipids involved in oncogenic signaling. Of note, ABHD6 has also been reported to act as the principle lipase responsible for 2-AG hydrolysis in cells lacking MAGL.[15] Thus, it would be of value to have a tailored-ABP to study the role of MAGL activity in oncogenic lipid signaling in cancer cells. This chapter reports on the discovery of a new ABP for MAGL that does not label ABHD6 and is used to visualize the subcellular localization of MAGL in MCF7 breast cancer cells and can be applied *in vivo*.

Results and discussion

Development of a highly selective activity-based probe for MAGL

Chemical probes **6** and **7** targeting MAGL were designed, based on compounds **4** and **5**, in which a para-chlorine substituent of the phenyl ring was replaced by a 2-azidoethanol group to enable ligation to an alkyne-containing fluorophore at a late stage. Compounds **6** and **7** were synthesized in 8 steps starting from commercially available building blocks (Scheme 1). In brief, treatment of **8** with sodium azide, subsequent mesylation of azido alcohol **9** and alkylation of 4-hydroxybenzaldehyde with **10** afforded intermediate **11**. Treatment of aldehyde **11** with *p*-chlorophenylmagnesiumbromide, followed by thionyl chloride treatment provided compound **13**, which was coupled to *tert*-butyl piperazine-1-carboxylate. Removal of Boc-protecting group using HCl in 1,4-dioxane gave the free amine **15** in quantitative yield. Finally, direct coupling with the corresponding alcohols of 1,1,1,3,3,3-hexafluoroisopropanol or *N*-hydroxysuccinimide yielded azide probes **6** and **7**.

The activity of compounds **6** and **7** was assessed in a real time, fluorescence-based natural substrate assay using membrane fractions of HEK293T cells transiently transfected with recombinant human MAGL.[16] JZL184 (**1**), which was used as a positive control, displayed a pIC_{50} of 7.7 ± 0.1 (Figure 2a). Compounds **6** and **7** were also potent inhibitors with pIC_{50} values of 8.0±0.1 and 7.2±0.2, respectively. Competitive ABPP, using the broad-spectrum serine hydrolase ABP FP-TAMRA, was employed to analyze the inhibitor activity and selectivity on endogenously expressed serine hydrolases in mouse brain (Figure 2b-d). Compounds **6** and **7** inhibited the labeling of MAGL with a pIC_{50} of 6.7±0.1 and 6.8±0.1, respectively (Figure 2b-d). ABHD6 was detected as the only off-target for compound **6** at 10 µM, while compound **7** inhibited labeling of ABHD6 and an additional unidentified off-target (Figure 2c, indicated by the arrow). Reaction of mouse

proteome treated with compounds **6** or **7** to a fluorophore (Cy5-alkyne) using click chemistry demonstrated labeling of the two MAGL splice forms.

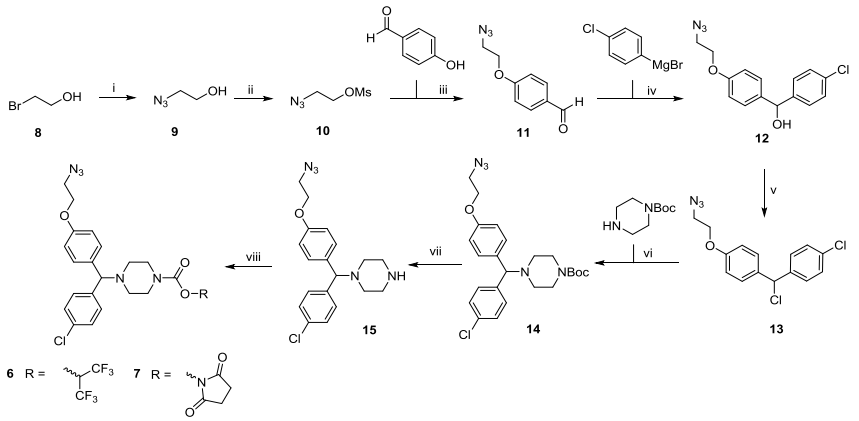

Scheme 1. Reagents and conditions: i) NaN_3, H_2O, 80 °C, 96%; ii) MsCl, TEA, DCM; iii) 4-hydroxybenzaldehyde, K_2CO_3, DMF, 80 °C, 86%; iv) 4-chlorophenyl magnesium bromide, THF, -78 °C, 89%; v) $SOCl_2$, DCM, 40 °C; vi) *tert*-butyl piperazine-1-carboxylate, K_2CO_3, DCM, 40 °C, 89%; vii) HCl in 1,4-dioxane, ethyl acetate; viii) corresponding alcohol, triphosgene, DIPEA, DCM, 54% (**6**), 87% (**7**).

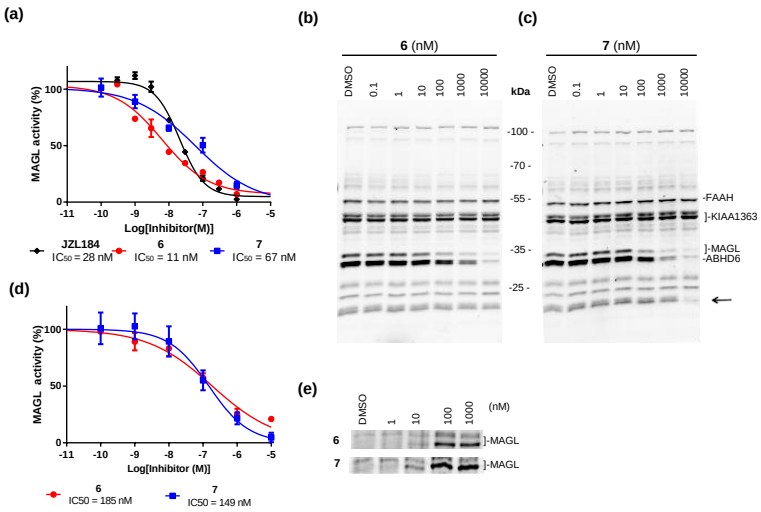

Figure 2. Activity and selectivity profile of MAGL inhibitors **6** and **7**. (a) Concentration-dependent inhibition curves of **6**, **7** and JZL184 (positive control) against hMAGL as determined with a natural substrate fluorescence assay (±SEM, n = 4); (b-c) Competitive ABPP with **6** (b) and **7** (c) (0.1 nM – 10000 nM) or vehicle (DMSO) in mouse brain membrane proteome using a broad-spectrum probe FP-TAMRA (500 nM, 20 min); (d) Concentration-dependent inhibition curves of **6** and **7** against endogenous MAGL as measured from gel (b) and (c) (±SEM, n = 3); (e) Two-step labeling of MAGL in mouse brain membrane proteome using **6** or **7** (1 – 1000 nM) followed by CuAAC reaction with alkyne-Cy5 tag (5 µM).

In view of its high selectivity profile, inhibitor **6** was conjugated to three different fluorophores: BODIPY-red, BODIPY-green and Cy5, which resulted in three different ABPs (**16**, **17** and **18,** respectively) (Figure 3a). All three probes were tested in the natural substrate assay and displayed a pIC_{50} of 5.5±0.4, 7.0±0.3 and 8.0±0.2, respectively (Figure 3b). The gel-based ABPP confirmed that probe **18** selectively and concentration-dependently labeled endogenous MAGL in mouse and rat brain proteomes (Figure 3c and 3d). MAGL activity was already visualized at low nanomolar concentrations and could be prevented by preincubation with JZL184 (Figure 4a). Surprisingly, competitive ABPP with FP-TAMRA and MB064 did not reveal any off-target activity for ABP **18**, including ABHD6 (Figure 4b,c). To further confirm the selectivity profile of ABP **18** over ABHD6, a real-time, fluorescence-based natural substrate assay was performed. Indeed, compound **18** did not inhibit ABHD6 up to 10 µM concentrations (Figure 4d). Collectively, these data show that ABP **18** serves as a potent and highly selective fluorescent probe for MAGL and is termed **LEI-463**.

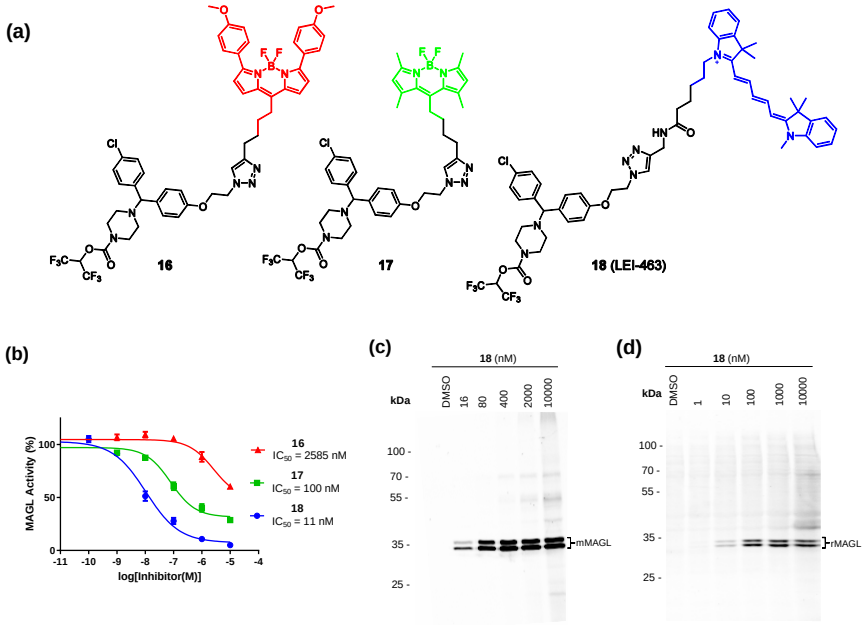

Figure 3. Development and characterization of fluorescent activity-based probes **16**-**18**. (a) Chemical structures of tailored-MAGL activity-based probes **16-18**; (b) Concentration-dependent inhibition curves of ABPs **16**-**18** against hMAGL as determined with 2-AG substrate assay, (±SEM, n=4); (c,d) Concentration-dependent labeling of MAGL activity with probe **18** (LEI-463) (30 min) in mouse (c) or rat (d) brain membrane proteome.

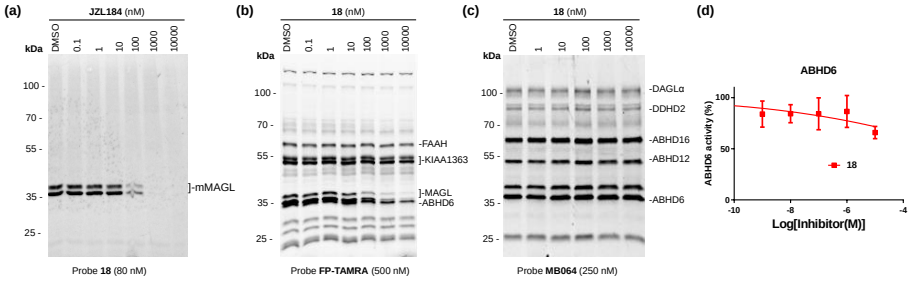

Figure 4. Selectivity profile of ABP **18** (LEI-463): (a) Competitive ABPP with MAGL inhibitor JZL184 (0.1-10000 nM) in mouse brain membrane proteome using **18** (80 nM; 30 min); (b,c) Competitive ABPP with **18** (0.1-10000 nM) in mouse brain proteome using probe FP-TAMRA (b) (500 nM, 20 min) or MB064 (c) (250 nM, 20 min); Of note, MB064 labels ABHD6 but not MAGL; (d) Concentration-dependent inhibition against hABHD6 by **18** as measured by 2-AG natural substrate assay (±SEM, n = 4).

Imaging of MAGL activity in cancer cells using LEI-463

Next, it was investigated whether LEI-463 can label MAGL in living cells. To this end, mouse neuroblastoma Neuro2A cells, which do not have endogenous MAGL activity,[17,18] were transiently transfected with a pcDNA3.1-construct in which MAGL is fused to Green Fluorescent Protein (eGFP). The cells were preincubated, 24h after transfection, with vehicle (DMSO), MAGL inhibitor JZL184 (10 µM) or ABHD6 inhibitor KT195 (10 µM) for 2h, and subsequently treated with LEI-463 (100 nM, 2h). Fluorescence microscopy was performed to study the co-localization of MAGL-eGFP (green colour) and LEI-463 labeling (red colour). Clear co-localization was observed in vehicle-treated cells, whereas JZL184, but not KT195, abolished MAGL labeling by LEI-463 (Figure 5a). Target engagement and selectivity of LEI-463 was confirmed in a gel-based ABPP experiment (Figure 5b-d). Together, these results indicate that LEI-463 is cell penetrable and selectively labels MAGL in living cells.

Next, it was assessed whether endogenous MAGL activity could be visualized by LEI-463 in breast cancer MCF7 cells.[10] Confocal fluorescent microscopy of MCF7 cells treated with LEI-463 (100 nM) showed a time-dependent increase in labeling of intracellular compartments, which could be prevented by pre-treatment of the cells with compound **6** (Figure 6a-b). Gel-based ABPP studies confirmed target engagement and selectivity of the probe in *in situ*-treated MCF7 cells (Figure 6c-e). Interestingly, prolonged incubation times (> 2h) at high concencentrations (> 100 nM) revealed an additional unidentified off-target with a molecular weight of 25 kDa, which could not be outcompeted by JZL184 or KT195.

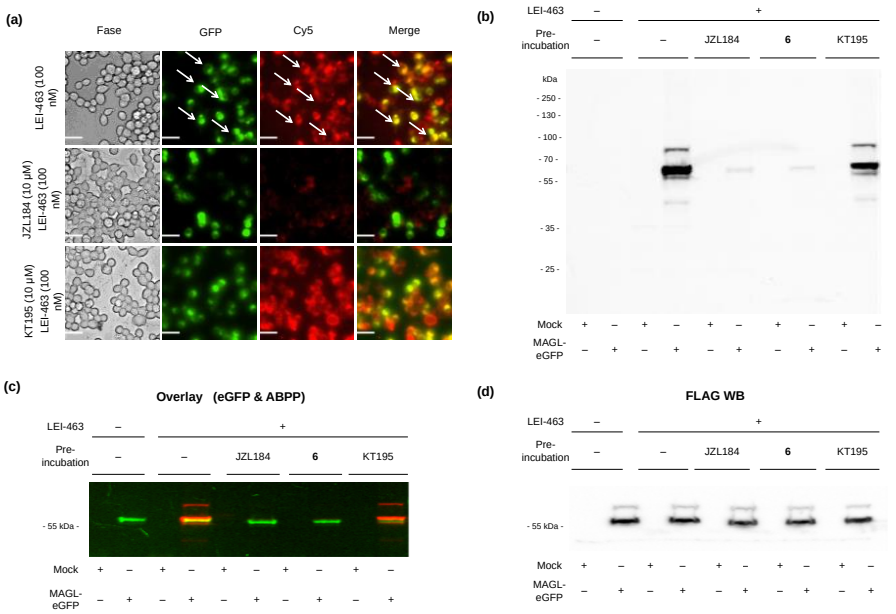

Figure 5. Imaging and labeling of recombinant MAGL-eGFP with probe LEI-463 in Neuro 2A cells. (a) Neuro2A cells transiently transfected with MAGL-eGFP were pre-incubated with vehicle (DMSO), JZL184 (10 µM) or ABHD6 inhibitor KT195 (10 µM) for 2h, followed by incubation with ABP LEI-463 (100 nM, 2h). Cells were washed with PBS (3x), and then used for fluorescent microscopy imaging. Arrows indicate representative examples of co-localization of MAGL-eGFP and probe labeled-MAGL. Scale bars: 50 µm; (b-c) MAGL-eGFP- or mock-transfected Neuro2A cells were pre-treated with MAGL inhibitors JZL184 or **6** (10 µM, 2h), KT195 (10 µM, 2h) or vehicle (DMSO), followed by treatment with probe LEI-463 (100 nM, 2h). After washing with PBS (3 x), cells were harvested and analyzed by gel-based ABPP. Scanning of the gel on Cy5 fluorescence shows probe labeling (b), and scanning on GFP fuorescence shows recombinant MAGL-eGFP signal (c); (d) MAGL-FLAG-eGFP expression levels in transfected Neuro2A cells as determined by anti-FLAG western blot.

To determine the subcellular membrane structures that contain MAGL activity in MCF7 cells, counterstaining experiments for LEI463-treated cells were performed with markers of various subcellular organelles, such as lyso-tracker that specifically stains acidic lysomosomes,[19-21] mito-tracker that contains a mildly thiol-reactive chloromethyl moiety for labeling mitochondria[22,23] and an ER-tracker that labels the endoplasmic reticulum.[24,25] Confocal imaging of LEI-463-treated cells on wavelengths specific to each marker revealed significant colocalization of MAGL activity with mitochondria and partial overlap with the ER, whereas very little co-localization with the punctate signals of lysosomes was found (Figure 7).

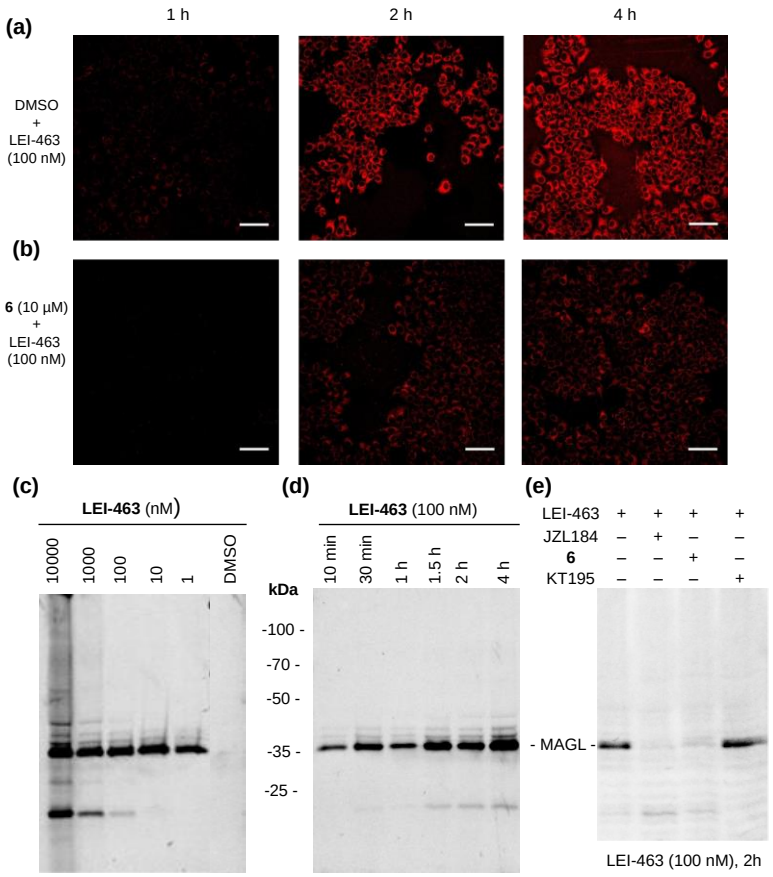

Figure 6. Detecting MAGL activity in cancer cells with probe LEI-463. (a,b) Confocal imaging of LEI-463-treated (100 nM) MCF7 cells with or without competitor **6** (10 µM); Laser setting: 20x lens; Cy5 channel: Gain: 754v, 18% intensity, excitation: 635 nm, emission: 660-700 nm; scale bar: 20 µm; (c,d) Gel analysis of LEI-463-treated MCF7 cells with various concentrations (c), and indicated incubation time (d); (e) Gel analysis of MCF7 cells treated with LEI-463 (100 nM, 2h) in presence or absence of following inhibitors: MAGL inhibitors JZL184 (10 µM, 2h), **6** (10 µM, 2h), or ABHD6 inhibitor KT195 (10 µM, 2h);

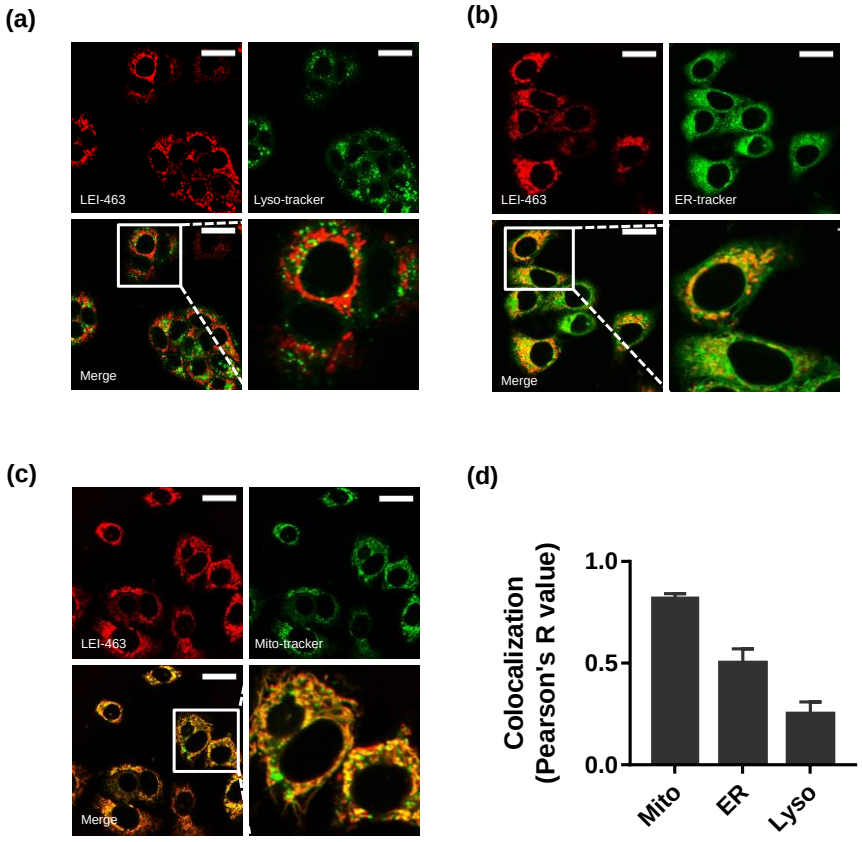

Figure 7. Subcellular localization of active MAGL in MCF7 cells with probe LEI-463 and various markers of subcellular organelles. MCF7 cells were treated with LEI-463 (100 nM, 2h), and stained with either lyso-tracker (a), ER-tracker (b), or mito-tracker (c) to visualize lysosomes, mitochondria and the endoplasmic reticulum respectively. After a PBS washing, the cells were used for confocal microscopy. Images show each fluorescence channel separately and the overlay of probe (Cy5, red) channel with lyso-marker (eGFP, green), ER-marker (DAPI, blue, false colored in image) or mito-marker channel (eGFP, green). Scale bar: 20 µm. (d) Colocalization of LEI-463 with lyso-, ER- or mito-marker was analyzed by Image J software (Coloc 2 plugin) using Pearson's R value (above threshold) as a measure; data represent average values ± SD; each experiment was repeated 3 times.

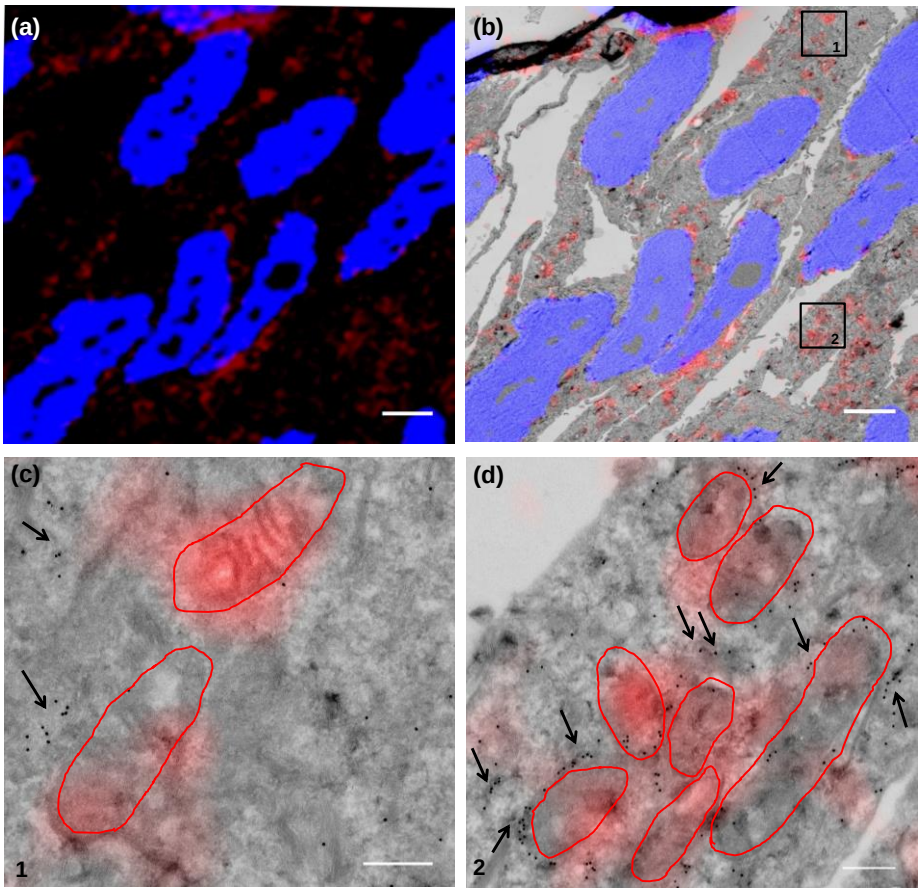

Figure 8. Correlative light-electron microscopy (CLEM) imaging of LEI-463 labeled MAGL in MCF7 cells. Cells were treated with LEI-463 (100 nM, 2 h) in 10 cm dish, followed by a PBS wash and immediate fixation. The fixed cells were harvested, subjected to Tokuyasu sample preparation, and cryosectioned into 75 nm sections. Sections were reacted with ER marker (anti-PDI) containing 15 nm gold particles (black dots in EM images, indicated with black arrows in c and d) and DAPI (blue) for nucleus. (a) Confocal microscopy images; (b) CLEM image obtained from overlay confocal microscopy and electron microscopy; (c) CLEM details from (b, region 1); (d) CLEM details from (b, region 2). Scale bar: 20 µm (a-b); 200 nm (c-d). Red circles in c and d indicate the locations of mitochondria from EM-images.

To confirm the subcellular localisation of MAGL activity at higher resolution, correlative light electron microscopy (CLEM) was performed. ABP-CLEM is a novel technology that allows one to correlate the activity of enzymes with the ultrastructural localisation of organelles as determined by electron microscopy (EM). LEI-463-treated MCF7 cells (100 nM, 2h) were fixated, cryosectioned according to the Tokuyasu-like sample preparation[26] and imaged. Confocal microscopy showed intracellular

fluorescence staining (Figure 8a) and subsequent correlation with EM-images of the same section revealed that MAGL activity resided to a large extent in mitochondria (indicated with red circles in Figure 8c-d). Considering the difficulty of visualizing ER structures in the cultured cells, an ER marker (anti-PDI with 15 nm gold particles) was used to detect the ER. The black dots indicated by the arrows in Figure 8c-d showed the subcellular localisation of the ER. The MAGL activity in the ER could not, however, unequivocally be established, due to the diffuse fluorescent signal and the close proximity of the ER and mitochondrial membranes (Figure 8d). Altogether, these experiments point towards the mitocondria as the principle subcellular compartment where MAGL activity resides in MCF7 cells.

LEI-463 labels MAGL *in vivo*

LEI-463 was further profiled *in vivo* to obtain tissue-wide MAGL activity and selectivity profile. LEI-463 (30 mg/kg, i.p.) or vehicle (saline/ethanol/PEG40, 18:1:1 (v/v/v)) was administrated to male C57BL/6 mice. After 2h or 4h, the animals were sacrificed and perfused with PBS and the organs (brain, heart, lung, liver, spleen, kidney, pancreas and testis) were isolated. Membrane and soluble proteomes of each tissue were prepared and analyzed by gel-based ABPP. No fluorescent bands were detected in any tissue after 2h of administration. At 4h a fluorescent band, corresponding to the molecular weight of MAGL (at ~33 kDa), was detected in all tissues except the brain (Figure 9), which indicated that LEI-463 is not brain penetrable. In testis, an additional band at ~35kDa was observed, which could represent the alternative splice variant of MAGL. Competitive ABPP with FP-TAMRA was performed to label residual MAGL activity. Near-complete blockade of MAGL activity was observed in all tissues, except the testis and the brain, indicating that almost full target engagement was obtained in heart, lung, liver, spleen, kidney and pancreas (Figure 9). LEI-463 maintained good selectivity for MAGL in most of the tissues, but several off-targets were detected in liver and pancreas (Figure 9b and 9g). The major off-targets of LEI-463 are around 50-65 kDa, which might correspond to carboxylesterases (CES), a subfamily of serine hydrolases that are commonly targeted by carbamate inhibitors. These in vivo studies, taken together, indicate that LEI-463 can be used to detect MAGL activity in intact animals and could function as a biomarker for target engagement.

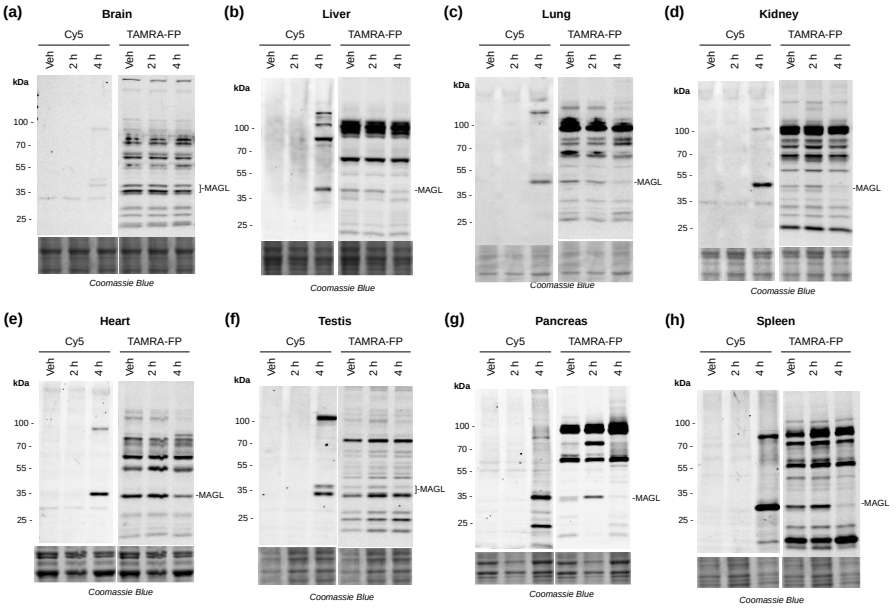

Figure 9. *In vivo* labeling of MAGL activity in mice. (a-h) C57Bl/6J mice were treated with LEI-463 (30 mg/kg) through intrapheritoneal injection for indicated time (2h or 4h), after which the animals were sacrificed and tissues, including brain (a), liver (b), lung (c), kidney (d), heart (e), testis (f), pancreas (g) and spleen (h), were harvested and analyzed for LEI-463-labeled proteins by gel-based fluorescence scanning. Scanning on Cy5 (left) and FP-TAMRA (*ex vivo*, 500 nM, 30 min) (right) channel confirmed the labeling of MAGL by LEI-463 *in vivo*.

Conclusion

This chapter describes the design, synthesis and application of a novel, highly selective and potent activity-based probe LEI-463 that visualizes MAGL activity in cell and tissue lysates as well as in living cells. It was discovered that MAGL activity is mainly localized in mitochondria of MCF7 cells. In addition, MAGL activity was detected in most mouse tissues, except the brain, after in vivo adminstration. It is envisioned that LEI-463 may serve as a valuable tailored ABP to study MAGL activity and distribution during (patho)physiological processes and may serve as a biomarker for target engagement studies to guide drug development.

Experimental section

Chemistry

All of reactions were performed using oven or flame-dried glassware and dry solvents. Reagents were purchased from Sigma Aldrich, Acros and Merck and used without further purification unless noted otherwise. All moisture sensitive reactions were performed under an argon atmosphere. Traces of water were removed from starting compounds by co-evaporation with toluene. ^{1}H-and ^{13}C-NMR spectra were recorded on a Bruker AV 400 MHz spectrometer at 400 (^{1}H) and 101 (^{13}C) MHz, or on a Bruker DMX-600 spectrometer 600 (^{1}H) and 150 (^{13}C) MHz using $CDCl_3$, or CD_3OD solvent, unless stated otherwise. Chemical shift values are reported in ppm with tetramethylsilane or solvent resonance as the internal standard ($CHCl_3$, δ 7.26 for ^{1}H, δ 77.16 for ^{13}C). Data are reported as follows: chemical shifts (δ), multiplicity (s = singlet, d = doublet, dd = double doublet, td = triple doublet, t = triplet, m = multiplet, br = broad), coupling constants *J* (Hz), and integration. High-resolution mass spectra (HRMS) were recorded by direct injection (2 µL of a 2 µM solution in water/acetonitrile 50/50 (v/v) and 0.1% formic acid) on a mass spectrometer (Thermo Finnigan LTQ orbitrap) equipped with an electrospray ion source in positive mode (source voltage 3.5 kV, sheath gas flow 10, capillary temperature 250 ^{o}C) with resolution R = 60,000 at m/z 400 (mass range m/z = 150-2,000) and dioctylphthalate (m/z = 391.28428) as a "lock mass". The high resolution mass spectrometer was calibrated prior to measurements with a calibration mixture (Thermo Finnigan). LC-MS analysis was performed on a Finnigan Surveyor HPLC system with a Gemmi C_{18} 50x4.60 mm column (detection at 200-600 nm), coupled to a Finnigan LCQ Adantage Max mass spectrometer with ESI. The applied buffers were H_2O, MeCN and 1.0% TFA in H_2O (0.1% TFA end concentration). Optical rotations were measured on a Propol automatic polarimeter (Sodium D-line, λ = 589 nm). Flash chromatography was performed using SiliCycle silica gel type SilicaFlash P60 (230 – 400 mesh). TLC analysis was performed on Merck silica gel 60/Kieselguhr F254, 0.25 mm. Compounds were visualized using either Seebach's reagent (a mixture of phosphomolybdic acid (25 g), cerium (IV) sulfate (7.5 g), H_2O (500 mL) and H_2SO_4 (25 mL)) or a $KMnO_4$ stain (K_2CO_3 (40 g), $KMnO_4$ (6 g), H_2O (600 mL) and 10% NaOH (5 mL)).

2-Azidoethan-1-ol (9). To a stirred solution of 2-bromoethan-1-ol (2 g, 16 mmol) in water (15 mL) was added sodium azide (2.6 g, 40 mmol), and the mixture was heated to 80 ^{o}C. After 15 h, KOH in pellets was added to basify the solution, followed by extraction with diethyl ether (3 x 20 mL). The combined organic phases were dried over $MgSO_4$. After filtration and removal of the solvent, 2-azidoethanol **9** was obtained as colorless liquid (1.34 g, 16 mmol, 96% yield). ^{1}H NMR (400 MHz, $CDCl_3$) δ 3.84 – 3.52 (m, 2H), 3.41 – 3.22 (m, 2H), 2.21 (br, 1H); ^{13}C NMR (101 MHz, $CDCl_3$) δ 61.51, 53.60.

2-Azidoethyl methanesulfonate (10). A solution of Ms-Cl (1.6 mL, 20.7 mmol) in DCM (5 mL) was added dropwise to a stirred solution of **9** (1.2 g, 13.8 mmol) and triethylamine (3.8 mL, 27.6 mmol) in DCM (15 mL) at 0 °C. After 2 h stirring at room temperature the reaction mixture was washed with water, dried over $MgSO_4$, filtered and evaporated to dryness to give title compound **10** as yellow oil, which was used directly without further purification. LC/MS calculated for $[C_3H_7N_3O_3S]^+$: 165.17, found: 165.92; ^{1}H NMR (400 MHz, $CDCl_3$) δ 4.39 – 4.11 (m, 1H), 3.52 (s, 1H), 3.00 (s, 1H); ^{13}C NMR (101 MHz, $CDCl_3$) δ 67.92, 49.60, 37.31.

4-(2-Azidoethoxy)benzaldehyde (11). 4-Hydroxybenzaldehyde (1.4 g, 11.6 mmol) and K_2CO_3 (2.4 g, 17.5 mmol) were added to a solution of 2-azidoethyl methanesulfonate (2.5 g, 15.1 mmol) in DMF (30 mL) at room temperature and the reaction mixture was stirred for 12 h at 80 ^oC. The resulting mixture was poured into water (30 mL) and extracted with diethyl ether (3 times). The combined organic layers were washed with brine (2 mL), dried over $MgSO_4$, filtered, and concentrated under reduced pressure. The residue was purified by flash column chromatography on silica gel with ethyl acetate/pentane (5−25%) as an eluent to yield **11** (1.9 g, 10 mmol, 86% yield). LC/MS calculated for $[C_9H_9N_3O_2]^+$: 191.19, found: 191.87; ^{1}H NMR (400 MHz, $CDCl_3$) δ 9.91 (s, 1H), 7.87 (d, *J* = 9.6 Hz, 2H), 7.04 (d, *J* = 8.4 Hz, 2H), 4.25 (t, *J* = 4.9 Hz, 2H), 3.67 (t, *J* = 4.8 Hz, 2H); ^{13}C NMR (101 MHz, $CDCl_3$) δ 190.85, 163.19, 132.09,130.48,114.88, 67.29, 50.03.

(4-(2-Azidoethoxy)phenyl)(4-chlorophenyl)methanol (12). To a stirring solution of **11** (1.2 g, 6.28 mmol) in dry THF (25 mL) at −78 °C under argon atmosphere was added (4-chlorophenyl)magnesium bromide (12.55 mL, 12.55 mmol) (1.0 M in diethyl ether). After 4 h, the reaction was quenched with saturated aqueous $NaHCO_3$ (5 mL) and the aqueous layer extracted with DCM (3 x 80 mL). The combined organic layers were dried over $MgSO_4$ and concentrated under reduced pressure. The residue was purified by flash chromatography (5−15% EtOAc/pentane) to give product **12** (1.7 g, 5.60 mmol, 89% yield). LC/MS calculated for $[C_{15}H_{14}ClN_3O_2]^+$: 303.75, found: 304.12; ^{1}H NMR (400 MHz, $CDCl_3$) δ 7.30 (s, 4H), 7.28 – 7.22 (m, 2H), 6.89 (d, *J* = 8.7 Hz, 2H), 5.77 (s, 1H), 4.13 (t, *J* = 5.0 Hz, 2H), 3.58 (t, *J* = 4.9 Hz, 2H), 2.22 (br, 1H). ^{13}C NMR (101 MHz, $CDCl_3$) δ 157.64, 142.40, 136.35, 132.88, 128.39, 127.87, 127.71, 114.50, 77.16, 74.79, 66.90, 49.98.

***tert*-Butyl**
4-((4-(2-azidoethoxy)phenyl)(4-chlorophenyl)methyl)piperazine-1-carboxylate
(14). To a stirring solution of **12** (800 mg, 2.63 mmol) in dry DCM (5 mL) at room temperature under argon atmosphere was added thionyl chloride (2.1 mL, 29 mmol). After stirred at 40 °C for overnight, the reaction was quenched with saturated aqueous $NaHCO_3$ (20 mL) and the aqueous layer extracted with DCM (3 × 10 mL). The combined organic layers were dried over $MgSO_4$, filtered and concentrated under reduced pressure to give crude product **13**, which was used for next step without further purification. To a solution of **13** (850 mg, 2.64 mmol) in DCM (12 mL) was added *tert*-butyl piperazine-1-carboxylate (1.5 g, 7.9 mmol) and K_2CO_3 (1.9 g, 13.7

mmol) at room temperature. After stirred at 40 °C for overnight, the reaction was quenched with saturated aqueous $NaHCO_3$ (20 mL) and the aqueous layer extracted with CH_2Cl_2 (3 × 10 mL). The combined organic layers were dried over Na_2SO_4 and concentrated under reduced pressure. The mixture was purified by flash chromatography (5−15% EtOAc/pentane) to give title compound **14** (1.2 g, 2.4 mmol, 89% yield). LC/MS calculated for $[C_{24}H_{30}ClN_5O_3]^+$: 471.99, found: 472.52; ^{1}H NMR (400 MHz, $CDCl_3$) δ 7.33 (d, *J* = 8.5 Hz, 2H), 7.29 – 7.21 (m, 4H), 6.84 (d, *J* = 8.7 Hz, 2H), 4.17 (s, 1H), 4.10 (t, *J* = 4.0 Hz, 2H) 3.56 (t, *J* = 5.0 Hz, 2H), 3.44 – 3.36 (m, 4H), 2.31 (br, 4H), 1.43 (s, 9H); ^{13}C NMR (101 MHz, $CDCl_3$) δ 157.51, 154.90, 141.39, 134.77, 132.71, 129.13, 129.09, 128.86, 114.81, 79.68, 74.69, 67.08, 51.72, 50.23, 44.38, 28.54.

1-((4-(2-Azidoethoxy)phenyl)(4-chlorophenyl)methyl)piperazine (15). To a solution of compound **14** (300 mg, 0.64 mmol) in ethyl acetate (2 mL) was added HCl (0.8 mL, 3.2 mmol) in 1,4-dioaxe. After TLC analysis indicated complete consumption of starting material, the mixture was poured into a saturated solution of $NaHCO_3$ and the product was extracted with DCM (3 x 20 mL). The combined organic layers were dried over $MgSO_4$, filtered and concentrated under reduced pressure to provide crude product **15**, which was used in the next step without further purification. LC/MS calculated for $[C_{19}H_{22}ClN_5O]^+$: 371.87, found: 372.64; ^{1}H NMR (400 MHz, $CDCl_3$) δ 7.63 – 7.09 (m, 6H), 6.84 (d, *J* = 8.6 Hz, 2H), 4.61 (br, 1H), 4.20 (s, 1H), 4.10 (t, *J* = 5.0 Hz, 2H), 3.55 (t, *J* = 8.0 Hz, 2H), 2.97 (t, *J* = 4.5 Hz, 4H), 2.44 (br, 4H); ^{13}C NMR (101 MHz, $CDCl_3$) δ 173.00, 157.42, 141.20, 134.55, 132.61, 129.04, 128.98, 128.76, 114.74, 74.87, 66.98, 51.85, 50.12, 45.53.

1,1,1,3,3,3-Hexafluoropropan-2-yl 4-((4-(2-azidoethoxy)phenyl)(4-chlorophenyl)methyl) piperazine-1-carboxylate (6). To a stirring solution of triphosgene (80 mg, 0.3 mmol) in CH_2Cl_2 (4 mL) at 0 ^{o}C was added the 1,1,1,3,3,3-hexafluoropropan-2-ol (0.062 mL, 0.59 mmol) followed by DIPEA (0.28 mL, 1.6 mmol). After stirring for 2h at room temperature, **15** (200 mg, 0.54 mmol) was added as a solution in CH_2Cl_2 (1 mL) and stirred for another 2 h. The mixture was concentrated under reduced pressure and purified by flash chromatography on silica gel (1−20% EtOAc/pentane) to provide the title compound **6** (165 mg, 0.29 mmol, 54% yield). HRMS calculated for $[C_{23}H_{22}ClF_6N_5O_3]^+$: 566.13881, found: 566.13875; ^{1}H NMR (400 MHz, $CDCl_3$) δ 7.33 (d, *J* = 8.4 Hz, 2H), 7.30 – 7.20 (m, 4H), 6.84 (d, *J* = 8.6 Hz, 2H), 5.74 (septet, *J* = 6.4 Hz, 1H), 4.20 (s, 1H), 4.09 (t, *J* = 4.9 Hz, 2H), 3.59 – 3.48 (m, 6H), 2.38 (dt, *J* = 14.2, 4.1 Hz, 4H); ^{13}C NMR (101 MHz, $CDCl_3$) δ 157.64, 151.44, 140.95, 134.27, 132.91, 129.02, 129.00, 128.95, 114.90, 74.46, 68.87 (q, *J* = 228 Hz), 68.08 (p, *J* = 35.4 Hz), 67.08, 51.36, 51.20, 50.18, 44.92, 44.56.

2,5-Dioxopyrrolidin-1-yl 4-((4-(2-azidoethoxy)phenyl)(4-chlorophenyl)methyl)piperazine-1- carboxylate (7). To a stirring solution of triphosgene (40 mg, 0.13 mmol) in DCM (5 mL) at 0 ^{o}C was added *N*-Hydroxysuccinimide (37 mg, 0.32 mmol) followed by DIPEA (0.14 mL,

0.81 mmol). After stirring for 2 h at room temperature, **15** (100 mg, 0.27 mmol) was added as a solution in DCM (1 mL) and stirred for another 2 h. The mixture was concentrated under reduced pressure and purified by flash chromatography on silica gel (1−20% EtOAc/pentane) to provide the title compound **7** (120 mg, 0.23 mmol, 87% yield). HRMS calculated for $[C_{24}H_{25}ClN_6O_5]^+$: 513.16477, found: 513.16478; ^{1}H NMR (400 MHz, $CDCl_3$) δ 7.34 (d, *J* = 8.4 Hz, 2H), 7.30 – 7.21 (m, 4H), 6.84 (d, *J* = 8.5 Hz, 2H), 4.22 (s, 1H), 4.18 – 4.01 (m, 2H), 3.68 – 3.44 (m, 6H), 2.78 (s, 4H), 2.42 (s, 4H); ^{13}C NMR (101 MHz, $CDCl_3$) δ 169.84, 157.59, 150.36, 140.94, 134.25, 132.85, 129.01, 128.99, 128.92, 114.88, 74.37, 67.04, 51.09, 51.03, 50.15, 45.25, 44.73, 25.54.

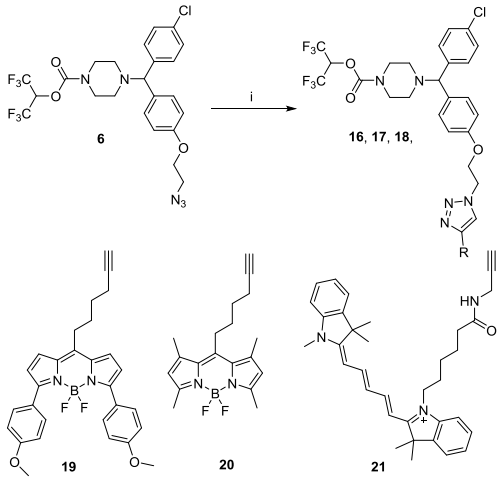

Scheme S.1. Synthesis of activity-based probe **16**-**18**. Reagents and conditions: (a) **19**, **20** or **21**, $CuSO_4$, sodium ascorbate, DCM/H_2O, r.t., 24 h, 69% (**16**), 61% (**17**) and 38% (**18**).

1,1,1,3,3,3-Hexafluoropropan-2-yl 4-((4-chlorophenyl)(4-(2-(4-(4-(5,5-difluoro-3,7-bis(4-methoxyphenyl)-*5H*-4l4,5l4-dipyrrolo[1,2-c:2',1'-f][1,3,2]diazaborinin-10-yl)butyl)-*1H*-1,2,3-triazol-1-yl)ethoxy)phenyl)methyl)piperazine-1-carboxylate (16). Compound **6** (38 mg, 0.07 mmol) and **19** (35 mg, 0.07 mmol) were dissolved in degassed DCM/H_2O (2 mL, 1:1, v/v) and aqueous solutions of sodium ascorbate (15.8 mg, 0.08 mmol) and copper(II) sulfate pentahydrate (8.3 mg, 0.03 mmol) were added. The resulting mixture was stirred vigorously for 2 h, after which TLC indicated completed conversion of the reaction. The solvents were evaporated *in vacuo*, and the residue was taken up in DCM and purified by silica column chromatography (1−5% DCM/MeOH) to give the desired product **16** (48 mg, 0.05 mmol, 69% yield). HRMS calculated for $[C_{52}H_{49}BClF_8N_7O_5]^+$ 1050.3522, found: 1050.3537; ^{1}H NMR (400 MHz, $CDCl_3$) δ 7.83 (d, *J* = 8.8 Hz, 4H), 7.33 – 7.14 (m, 9H), 6.93 (d, *J* = 8.9 Hz, 4H), 6.75 (d, *J* = 8.2 Hz, 2H), 6.58 (s, 2H), 5.72 (septet, *J* = 6.4 Hz, 1H), 4.71 (s, 2H), 4.31 (s,

2H), 4.15 (s, 1H), 3.83 (s, 6H), 3.52 (d, *J* = 5.0 Hz, 4H), 2.96 (s, 2H), 2.78 (br, 1H), 2.34 (dt, *J* = 12.2, 4.5 Hz, 4H), 1.87 (br, 4H). ^{13}C NMR (101 MHz, $CDCl_3$) δ 160.67, 157.66, 157.21, 151.42, 144.87, 140.81, 136.26, 134.68, 132.95, 131.14, 131.09,131.04, 129.05, 128.98, 128.97, 125.29, 122.17, 120.12, 114.87, 113.84, 74.35, 69.08 (q, *J* = 224.2 Hz), 68.09 (p, *J* = 35.35 Hz), 66.42, 55.36, 51.32, 51.16, 50.29, 44.88, 44.53, 33.12, 31.70, 30.52.

1,1,1,3,3,3-Hexafluoropropan-2-yl 4-((4-chlorophenyl)(4-(2-(4-(4-(5,5-difluoro-1,3,7,9-tetramethyl-*5H*-4l4,5l4-dipyrrolo[1,2-c:2',1'-f][1,3,2]diazaborinin-10-yl)butyl)-*1H*-1,2,3-triazol-1-yl)ethoxy)phenyl)methyl)piperazine-1-carboxylate (17). The title compound was synthesized from compound **6** (33 mg, 0.06 mmol), **20** (21 mg, 0.06 mmol), sodium ascorbate (13.9 mg, 0.07 mmol) and copper(II) sulfate pentahydrate (7.3 mg, 0.03 mmol) according to the procedure described for compound **16**. This furnished the title compound **17** (32 mg, 0.04 mmol, 61% yield). HRMS calculated for $[C_{42}H_{45}BClF_8N_7O_3]^+$ 894.33105, found: 894.33253; ^{1}H NMR (400 MHz, $CDCl_3$) δ 7.45 (s, 1H), 7.31 (d, *J* = 8.4 Hz, 2H), 7.29 – 7.20 (m, 5H), 6.77 (d, *J* = 8.5 Hz, 2H), 6.02 (s, 2H), 5.72 (septet, *J* = 6.4 Hz, 1H), 4.70 (s, 2H), 4.29 (s, 2H), 4.19 (s, 1H), 3.63 – 3.42 (m, 4H), 2.97 (br, 2H), 2.77 (s, 2H), 2.50 (s, 6H), 2.37 (s, 10H), 1.91 (s, 2H), 1.68 (br, 4H). ^{13}C NMR (101 MHz, $CDCl_3$) δ 157.24, 153.98, 153.95, 151.46, 146.18, 140.84, 140.46, 140.45, 134.76, 133.02, 129.08, 129.02, 129.00, 121.81, 121.76, 114.90, 74.41, 68.66 (q, *J* = 244.4 Hz), 68.12 (p, *J* = 34.34 Hz), 66.54, 51.38, 51.21, 49.89, 44.91, 44.55, 31.48, 29.49, 28.25, 25.52, 16.48, 14.55.

1-(6-(((1-(2-(4-((4-Chlorophenyl)(4-(((1,1,1,3,3,3-hexafluoropropan-2-yl)oxy)carbonyl)piperazin-1-yl)methyl)phenoxy)ethyl)-*1H*-1,2,3-triazol-4-yl)methyl)amino)-6-oxohexyl)-3,3-dimethyl-2-((1*E*,3*E*)-5-((*E*)-1,3,3-trimethylindolin-2-ylidene)penta-1,3-dien-1-yl)-*3H*-indol-1-ium chloride (18, LEI-463). The title compound was synthesized from compound **6** (10 mg, 0.018 mmol), **21** (9.8 mg, 0.018 mmol), sodium ascorbate (4.20 mg, 0.021 mmol) and copper(II) sulfate pentahydrate (2.2 mg, 8.8 µmol) according to the procedure described for compound **16**. This furnished the title compound **18** (7.6 mg, 0.007 mmol, 38% yield). HRMS calculated for $[C_{58}H_{64}ClF_6N_8O_4]^+$ 1085.46378, found: 1085.46335; ^{1}H NMR (600 MHz, $CDCl_3$) δ 7.86 (d, *J* = 10.1 Hz, 2H), 7.42 – 7.32 (m, 4H), 7.26 (s, 8H), 7.10 – 7.08 (m, 2H), 6.99 – 6.72 (m, 4H), 6.38 (br d, *J* = 45.0 Hz, 2H), 5.76 – 5.65 (m, 1H), 4.76 (br, 4H), 4.34 (br, 3H), 4.04 (s, 3H), 3.78 – 3.44 (m, 6H), 2.53 – 2.23 (m, 4H), 1.83 – 1.54 (m, 18H), 1.25 (s, 2H). ^{13}C NMR (151 MHz, $CDCl_3$) δ 173.02, 158.94, 153.36, 152.92, 151.35, 142.86, 142.03, 141.16, 140.88, 128.96, 128.85, 125.48, 125.24, 122.32, 122.23, 110.96, 110.48, 70.29 (q, *J* = 285.4 Hz), 68.13 (p, *J* = 36.2 Hz), 67.92, 66.38, 64.35, 51.47, 51.34, 49.44, 49.20, 45.11, 29.85, 28.30, 28.25, 27.35.

Biological assays

Cloning Procedures

For the preparation of the different constructs, full length human cDNA was purchased from Source Bioscience and cloned into mammalian expression vector pcDNA3.1, containing genes for ampicillin and neomycin resistance. MAGL constructs were obtained as reported previously [27]. Plasmids were isolated from transformed XL-10 Z-competent cells (Maxi Prep, Qiagen) and verified by Sanger sequencing (BaseClear). The sequences were confirmed by sequence analysis at the Leiden Genome Technology Centre.

Cell culture and membrane preparation

Cells (HEK293T, Neuro2A) were grown in DMEM with stable glutamine and phenolred (PAA or Sigma) with 10% New Born Calf serum, penicillin and streptomycin. Cells were passaged every 2-3 days by resuspending (HEK293T, Neuro2A) in medium and seeding them to appropriate confluence. Membranes were prepared from transiently transfected cells. One day prior to transfection 10^7 cells were seeded in a 15 cm petri dish. Cells were transfected by the addition of a 3:1 mixture of polyethyleneimine (60 µg) and plasmid DNA (20 µg) in 2 mL serum free medium. The medium was refreshed after 24 h, and after 72 h the cells were harvested by suspending them in 20 mL medium. The suspension was centrifuged for 10 min at 1000 rpm, and the supernatant was removed. The cell pellet was stored at -80 ^{o}C until use. Of note, Neuro2A cells were transfected by the addition of a 5:1 mixture of polyethyleneimine (5 µg) and plasmid DNA (1 µg) in serum free medium in 6-well plate.

Cell pellets were thawed on ice and suspended in lysis buffer A (20 mM HEPES, 2 mM DTT, 0.25 M sucrose, 1 mM $MgCl_2$, 25 U/mL Benzonase). The suspension was homogenized by polytrone (3 × 7 sec) and incubated for 30 min on ice. The suspension was subjected to ultracentrifugation (93.000 × g, 30 min, 4 ^{o}C, Beckman Coulter, Type Ti70 rotor) to yield the cytosolic fraction in the supernatant and the membrane fraction as a pellet. The pellet was resuspended in lysis buffer B (20 mM HEPES, 2 mM DTT). The protein concentration was determined with Quick Start Bradford reagent (BioRad) or Qubit^{TM} fluorometric quantitation (Life Technologies). The protein fractions were diluted to 1 mg/mL and stored in small aliquots at -80 ^{o}C until use.

Live-cell microscopy

Experiments were conducted on a Leica TCS SPE confocal microscope, using Cy5 filter setting (λex: 633 nm, λem: 660-700 nM). MCF7 cells (1-2 x 10^4) were seeded onto sterile µ-Slide 8 well coverglass (I bidi). Stock solutions of probes and other reagents in DMSO (0.1%) were diluted with medium without serum. Cells were incubated with probe LEI-463 for 2 h and then subsequently washed with PBS (3x), fixed (4% formaldehyde in PBS; 15 min at r.t.), washed again with PBS (3x). Fixed

cells were then used for fluorescent imaging. For the competition experiments, MAGL inhibitors JZL184 or ABHD6 inhibitor KT195 were *in situ* pre-incubated for 2 h prior and then co-incubated with probe LEI-463 for another 2 h. For the co-localization experiments, after treatment with probe LEI-463 for 2 h, cells were washed with PBS (3x), and then stained with lyso-tracker Green DND26 (Thermo Fisher; 1 µM), Mito-tracker Green FM (Thermo Fisher; 200 nM) or ER-tracker Blue-White DPX (Thermo Fisher 1 µM) according to manufacturer's recommendations for 30 min at 25 ^{o}C. For the co-localization studies, Pearson's correlation coefficient was measured by Image J software with Coloc 2 plugin. Each staining experiment was repeated 3 times.

Correlation of light-electron microscopy (CLEM)

The CLEM approach used was adapted from Van Elsland et. al.[28] Samples were prepared for cryo sectioning as described elsewhere.[29] MCF-7 cells were incubated with the LEI-463 probe for 2 h. After the probe incubation cells were washed with PBS (3x) and were then fixed for 24h in freshly prepared 2% PFA in 0.1 M phosphate buffer. Fixed cells were embedded in 12% gelatin (type A, bloom 300, Sigma) and cut with a razor blade into 0.5 mm^3 cubes. The sample blocks were infiltrated in phosphate buffer containing 2.3 M sucrose for 3h. Sucrose-infiltrated sample blocks were mounted on aluminum pins and plunged in liquid nitrogen. The frozen samples were stored under liquid nitrogen.

Ultrathin cell sections of 75 nm were obtained as described elsewhere.[28] Briefly, the frozen sample was mounted in a cryo-ultramicrotome (Leica). The sample was trimmed to yield a squared block with a front face of about 300 x 250 µm (Diatome trimming tool). Using a diamond knife (Diatome) and antistatic devise (Leica) a ribbon of 75 nm thick sections was produced that was retrieved from the cryo-chamber with a droplet of 2.3 M sucrose. Obtained sections were transferred to a specimen grid previously coated with formvar and carbon Grids were additionally coated as indicated with either 100 nm TetraSpeck beads or 100 nm FluoroSpheres (blue) carboxylate-modified (350/440) (Life Technologies).

Obtained sample sections were subsequently immunogold-labeled with 15 nm gold particles using a rabbit anti-protein disulfide isomerase (PDI) polyclonal antibody.[30] Sections were labeled as follows; thawed cryo sections on an EM grid were left for 30 minutes on the surface of 2% gelatin in phosphate buffer at 37 °C. Grids were washed 5 times with PBS/glycine and blocked with PBS/Glycine containing 1% BSA after which the grids were incubated for 1h with PBS/Glycine 1% BSA supplemented with anti-PDI.[30] Grids were then washed 5 times with PBS/glycine and blocked with PBS/Glycine 0.1% BSA, grids were incubated for 20 min on PBS/Glycine 1% BSA supplemented with protein A coated 15 nm gold particles (CMC, Utrecht University). Grids were then washed with PBS, labeled with DAPI (1:5000 in PBS for 5 min), and additionally washed with PBS and aquadest.

Grids containing the sample sections were then washed with 50% glycerol and

placed on glass slides (pre- cleaned with 100% ethanol). Grids were then covered with a small drop of 50% glycerol after which a coverslip was mounted over the grid. Coverslips were fixed using Scotch Pressure Sensitive Tape. Samples were imaged with a Leica TCS SP8 confocal microscope (63x oil lens, N.A.=1.4). Confocal microscopy was used as it allowed to make image stacks from the sections at different focus planes, this was convenient as the sections were found to be in different focus planes whilst placed between the glass slides and coverslip. After fluorescence microscopy the EM grid with the sections was remove from the glass slide, rinsed in distilled water and incubated for 5' on droplets of unranylacetate/methylcellulose. Excess of uranylacetate/methylcellulose was blotted away and grids were air-dried. EM imaging was performed with an Tecnai 12 Biotwin transmission electron microscope (FEI) at 120 kV acceleration voltage. Correlation of confocal and EM images was performed in Adobe Photoshop CS6. In Adobe Photoshop, the LM image was copied as a layer into the EM image and made 50% transparent. Transformation of the LM image was necessary to match it to the larger scale of the EM image. This was performed via isotropic scaling and rotation. Interpolation settings; bicubic smoother. Alignment at low magnification was carried out with the aid of nuclear DAPI staining in combination with the shape of the cells, at high magnification alignment was performed using the fiducial beads.

Natural substrate based fluorescence assay (MAGL and ABHD6)

The natural substrate assays were performed as reported previously.[27, 31] Standard assay conditions: 0.2 U/mL glycerol kinase (GK), glycerol-3-phosphate oxidase (GPO) and horseradish peroxidase (HRP), 0.125 mM ATP, 10 µM Amplifu™Red, 5% DMSO in a total volume of 200 µL. For ABHD6, the assay additionally contained 25 µM 2-AG and 0.5% acetonitrile, with a final protein concentration of 40 µg/mL.

Preparation of mouse tissue membrane proteome

Mouse tissues were isolated according to guidelines approved by the ethical committee of Leiden University (DEC#13191), frozen in liquid nitrogen and stored at -80 °C until use. Mouse tissues were thawed on ice and homogenized by polytrone (3 x 5 seconds, 20,000 rpm) in lysis buffer A (20 mM HEPES pH 7.2, 2 mM DTT, 250 mM sucrose, 1 mM $MgCl_2$ and 25 U/mL benzonase). The suspension was incubated on ice for 15 min, followed by low speed centrifugation (2500 g, 3 min. at 4 °C) to remove debris. The supernatant was subjected to ultracentrifugation (93,000 g, 45 min at 4 °C) to yield the mouse tissue membrane proteome as a pellet. The pellet was resuspended in storage buffer B (20 mM HEPES, pH 7.2, 2 mM DTT) and homogenized by polytrone (1 x 7 seconds, 20,000 rpm). Protein concentrations were determined and membranes preparations were stored as described above.

Activity based protein profiling in mouse brain.

Mouse brain proteome (2 mg/mL, 19.5 µL) was incubated with DMSO or inhibitor in 0.5 µL DMSO for 30 min at r.t. and subsequently incubated with 500 nM (final

concentration) ABP FP-TAMRA, or 250 nM (final concentration) ABP MB064 for 20 min at r.t. before the reaction was quenched with standard 3x Laemmli sample buffer. The gels were scanned using a ChemiDoc MP system and analyzed using Image Lab 4.1.

Activity-based protein profiling in living cells

Breast cancer cell MCF7 were grown in DMEM with stable glutamine and phenolred (PAA), 10% New Born Calf serum, penicillin and streptomycin. Cells were passaged every 2-3 days by resuspension (trypsinization) in medium and seeing them to appropriate confluence. Before inhibitor treatment, the culture medium was removed and the cells were washed with warm (37 ^{o}C) serum-free medium (3x). For labeling experiments, cells were treated with DMSO or various concentrations of probe LEI-463 (1000x DMSO stock; final DMSO concentration 0.1%), incubated for 2 h (37 ^{o}C; 5% CO_2), washed with PBS (3x) and harvested (trypsinization). Cell pellets were flash frozen in liquid nitrogen before ABPP analysis. Experiments that required pre-treatment were conducted as follows: the cells were incubated with DMSO or inhibitor (1000x DMSO stock; final DMSO concentration 0.1%) in serum-free medium for 2 h. The medium was removed and the cells were washed with PBS (3x). Probe LEI-463 (100 nM) was added directly to the medium and incubated for 2 h. After washing with PBS (3x), the cells were suspended in PBS and the cells were pelleted by centrifugation. Cell pellets were flash frozen in liquid nitrogen before analysis by ABPP.

***In vivo* target engagement studies of LEI-463**

The animal experiments were conducted in accordance with the ethical committee of Leiden University (DEC#14137). *In vivo* studies with LEI-463 were conducted in C57BL/6 mice. Mice were injected with LEI-463 (30 mg/kg) i.p. in 18:1:1 (v/v/v) solution of saline/ethanol/PEG40 (ethoxylated castor oil, 10 µL/g body weight of mouse). After 2 h or 4 h, mice were anesthetized with isoflurane, and euthanized by cervical dislocation. Mice were perfused with PBS and then brain, liver, spleen, heart, lung, pancreas, testis, muscle and kidney were collected. Tissue homogenates were prepared and competitive ABPP experiments were performed according to the previously described method.

References

1. Niphakis, M. J.; Cravatt, B. F. Enzyme inhibitor discovery by activity-based protein profiling. *Annual Review Biochemistry* **2014,** 83, 341-377.
2. Liu, Y. S.; Patricelli, M. P.; Cravatt, B. F. Activity-based protein profiling: The serine hydrolases. *Proceedings of the National Academy of Sciences of the United States of America* **1999,** 96, 14694-14699.
3. Adam, G. C.; Sorensen, E. J.; Cravatt, B. F. Proteomic profiling of mechanistically distinct enzyme classes using a common chemotype. *Nature Biotechnology* **2002,** 20, 805-809.
4. Greenbaum, D.; Baruch, A.; Hayrapetian, L.; Darula, Z.; Burlingame, A.; Medzihradszky, K. F.; Bogyo, M. Chemical approaches for functionally probing the proteome. *Molecular & Cellular Proteomics* **2002,** 1, 60-68.
5. Kumar, S.; Zhou, B.; Liang, F. B.; Wang, W. Q.; Huang, Z. H.; Zhang, Z. Y. Activity-based probes for protein tyrosine phosphatases. *Proceedings of the National Academy of Sciences of the United States of America* **2004,** 101, 7943-7948.
6. Patricelli, M. P.; Szardenings, A. K.; Liyanage, M.; Nomanbhoy, T. K.; Wu, M.; Weissig, H.; Aban, A.; Chun, D.; Tanner, S.; Kozarich, J. W. Functional interrogation of the kinome using nucleotide acyl phosphates. *Biochemistry* **2007,** 46, 350-358.
7. Vocadlo, D. J.; Bertozzi, C. R. A strategy for functional proteomic analysis of glycosidase activity from cell lysates. *Angewandte Chemie International Edition* **2004,** 43, 5338-5342.
8. Sieber, S. A.; Niessen, S.; Hoover, H. S.; Cravatt, B. F. Proteomic profiling of metalloprotease activities with cocktails of active-site probes. *Nature Chemical Biology* **2006,** 2, 274-281.
9. Niphakis, M. J.; Cravatt, B. F. Enzyme inhibitor discovery by activity-based protein profiling. *Annual Review of Biochemistry,* **2014,** 83, 341-377.
10. Nomura, D. K.; Long, J. Z.; Niessen, S.; Hoover, H. S.; Ng, S. W.; Cravatt, B. F. Monoacylglycerol lipase regulates a fatty acid network that promotes cancer pathogenesis. *Cell* **2010,** 140, 49-61.
11. Verdoes, M.; Florea, B. I.; Menendez-Benito, V.; Maynard, C. J.; Witte, M. D.; Van der Linden, W. A.; Van den Nieuwendijk, A. M. C. H.; Hofmann, T.; Berkers, C. R.; van Leeuwen, F. W. B.; Groothuis, T. A.; Leeuwenburgh, M. A.; Ovaa, H.; Neefjes, J. J.; Filippov, D. V.; Van der Marel, G. A.; Dantuma, N. P.; Overkleeft, H. S. A fluorescent broad-spectrum proteasome inhibitor for labeling proteasomes in vitro and in vivo. *Chemistry & Biology* **2006,** 13, 1217-1226.
12. Chang, J. W.; Moellering, R. E.; Cravatt, B. F. An activity-based imaging probe for the integral membrane hydrolase KIAA1363. *Angewandte Chemie International Edition* **2012,** 51, 966-970.
13. Dinh, T. P.; Carpenter, D.; Leslie, F. M.; Freund, T. F.; Katona, I.; Sensi, S. L.; Kathuria, S.; Piomelli, D. Brain monoglyceride lipase participating in endocannabinoid inactivation. *Proceedings of the National Academy of Sciences of the United States of America* **2002,** 99, 10819-10824.
14. Nomura, D. K.; Morrison, B. E.; Blankman, J. L.; Long, J. Z.; Kinsey, S. G.; Marcondes, M. C. G.; Ward, A. M.; Hahn, Y. K.; Lichtman, A. H.; Conti, B.; Cravatt, B. F. Endocannabinoid

hydrolysis generates brain prostaglandins that promote neuroinflammation. *Science* **2011,** 334, 809-813.

15. Marrs, W. R.; Blankman, J. L.; Horne, E. A.; Thomazeau, A.; Lin, Y. H.; Coy, J.; Bodor, A. L.; Muccioli, G. G.; Hu, S. S. J.; Woodruff, G.; Fung, S.; Lafourcade, M.; Alexander, J. P.; Long, J. Z.; Li, W. W.; Xu, C.; Moller, T.; Mackie, K.; Manzoni, O. J.; Cravatt, B. F.; Stella, N. The serine hydrolase ABHD6 controls the accumulation and efficacy of 2-AG at cannabinoid receptors. *Nature Neuroscience* **2010,** 13, 951-967.
16. Navia-Paldanius, D.; Savinainen, J. R.; Laitinen, J. T. Biochemical and pharmacological characterization of human alpha/beta-hydrolase domain containing 6 (ABHD6) and 12 (ABHD12). *Journal of Lipid Research* **2012,** 53, 2413-2424.
17. Shankavaram, U. T.; Reinhold, W. C.; Nishizuka, S.; Major, S.; Morita, D.; Chary, K. K.; Reimers, M. A.; Scherf, U.; Kahn, A.; Dolginow, D.; Cossman, J.; Kaldjian, E. P.; Scudiero, D. A.; Petricoin, E.; Liotta, L.; Lee, J. K.; Weinstein, J. N. Transcript and protein expression profiles of the NCI-60 cancer cell panel: an integromic microarray study. *Molecular Cancer Therapeutics* **2007,** 6, 820-832.
18. Hsu, K. L.; Tsuboi, K.; Adibekian, A.; Pugh, H.; Masuda, K.; Cravatt, B. F. DAGLbeta inhibition perturbs a lipid network involved in macrophage inflammatory responses. *Nature Chemical Biology* **2012,** 8, 999-1007.
19. Anderson, R. G. W.; Orci, L. A view of acidic intracellular compartments. *Journal of Cell Biology* **1988,** 106, 539-543.
20. Dolman, N. J.; Kilgore, J. A.; Davidson, M. W. A review of reagents for fluorescence microscopy of cellular compartments and structures, part I: BacMam labeling and reagents for vesicular structures. *Current Protocols in Cytometry* **2013,** Chapter 12, Unit 12 30.
21. Li, Y.; Zhang, Q.; Tian, R.; Wang, Q.; Zhao, J. J.; Iglehart, J. D.; Wang, Z. C.; Richardson, A. L. Lysosomal transmembrane protein LAPTM4B promotes autophagy and tolerance to metabolic stress in cancer cells. *Cancer Research* **2011,** 71, 7481-7489.
22. Buckman, J. F.; Hernandez, H.; Kress, G. J.; Votyakova, T. V.; Pal, S.; Reynolds, I. J. MitoTracker labeling in primary neuronal and astrocytic cultures: influence of mitochondrial membrane potential and oxidants. *Journal of Neuroscience Methods* **2001,** 104, 165-176.
23. Peng, T.; Bonamy, G. M. C.; Glory-Afshar, E.; Rines, D. R.; Chanda, S. K.; Murphy, R. F. Determining the distribution of probes between different subcellular locations through automated unmixing of subcellular patterns. *Proceedings of the National Academy of Sciences of the United States of America* **2010,** 107, 2944-2949.
24. Abodeely, M.; DuBois, K. N.; Hehl, A.; Stefanic, S.; Sajid, M.; deSouza, W.; Attias, M.; Engel, J. C.; Hsieh, I.; Fetter, R. D.; McKerrow, J. H. A contiguous compartment functions as endoplasmic reticulum and endosome/lysosome in Giardia lamblia. *Eukaryotic Cell* **2009,** 8, 1665-1676.
25. Mironov, S. L.; Ivannikov, M. V.; Johansson, M. [Ca2+](i) signaling between mitochondria and endoplasmic reticulum in neurons is regulated by microtubules - From mitochondrial permeability transition pore to Ca2+-induced Ca2+ release. *Journal of Biological Chemistry* **2005,** 280, 715-721.
26. Maranto, A. R. Neuronal mapping: a photooxidation reaction makes Lucifer yellow useful for electron microscopy. *Science* **1982,** 217, 953-955.

27. van der Wel, T.; Janssen, F. J.; Baggelaar, M. P.; Deng, H.; den Dulk, H.; Overkleeft, H. S.; van der Stelt, M. A natural substrate-based fluorescence assay for inhibitor screening on diacylglycerol lipase alpha. *Journal of Lipid Research* **2015,** 56, 927-935.
28. van Elsland, D. M.; Bos, E.; de Boer, W.; Overkleeft, H. S.; Koster, A. J.; van Kasteren, S. I. Detection of bioorthogonal groups by correlative light and electron microscopy allows imaging of degraded bacteria in phagocytes. *Chemical Science* **2016,** 7, 752-758.
29. Peters, P. J.; Hunziker, W. Subcellular localization of Rab17 by cryo-immunogold electron microscopy in epithelial cells grown on polycarbonate filters. *Regulators and Effectors of Small Gtpases, Pt E* **2001,** 329, 210-225.
30. McGehee, A. M.; Dougan, S. K.; Klemm, E. J.; Shui, G. H.; Park, B.; Kim, Y. M.; Watson, N.; Wenk, M. R.; Ploegh, H. L.; Hu, C. C. A. XBP-1-Deficient plasmablasts show normal protein folding but altered glycosylation and lipid synthesis. *Journal of Immunology* **2009,** 183, 3690-3699.
31. Janssen, F. J.; Deng, H.; Baggelaar, M. P.; Allara, M.; van der Wel, T.; den Dulk, H.; Ligresti, A.; van Esbroeck, A. C.; McGuire, R.; Di Marzo, V.; Overkleeft, H. S.; van der Stelt, M. Discovery of glycine sulfonamides as dual inhibitors of sn-1-diacylglycerol lipase alpha and alpha/beta-hydrolase domain 6. *Journal of Medicinal Chemistry* **2014,** 57, 6610-6622.